

# Design, synthesis, antitumor evaluation, 3D-QSAR and molecular docking studies of novel 4-aminoacridone compounds

Lin Tian<sup>1,2</sup> · Chang J. Feng<sup>2</sup> · Tong X. Li<sup>3</sup> · Zhao Li<sup>2</sup> · Wei H. Yang<sup>4</sup> · Xiang E. Han<sup>1</sup>

Received: 31 January 2016 / Accepted: 3 June 2017  
© Springer Science+Business Media, LLC 2017

**Abstract** 4-aminoacridone was efficiently synthesized using an optimized method and condensed with a variety of different aldehydes to give the corresponding Schiff bases, **1a–k**. The antiproliferative activities of these compounds were measured against several human cancer cell lines in vitro, including A549, HeLa, SGC-7901, and Raji cells. The results of these bioassays indicate that these compounds possess antiproliferative activity for the HeLa and Raji cell lines. In particular, compounds **1d** and **1k** containing 4-(*N,N*-dimethyl)phenyl and 2,4-dichlorophenyl groups, respectively, showed greater potency and selectivity towards HeLa cells than any of the other cell lines ( $IC_{50} = 7.75$  and  $8.88 \mu\text{M}$ , respectively). Three-dimensional contour maps based on highly predictive 3D-quantitative structure–activity relationship studies ( $R^2_{cv} = 0.674$ ,  $R = 0.956$ ) are used to explain the structure-activity relationships of these compounds. Furthermore, docking studies

were conducted to evaluate the multidrug resistance modulatory effects of these imine compounds in the adenosine tri-phosphate binding site of P-glycoprotein and the transmembrane binding pocket. These docking experiments revealed the occurrence of important interactions between these molecules and the active site of the transmembrane binding pocket, predicting multidrug resistance modulatory behavior.

**Keywords** 4-aminoacridone derivative · Antitumor activity · 3D-QSAR · Multidrug resistance (MDR) modulator · Docking analysis

**Electronic supplementary material** The online version of this article (doi:10.1007/s00044-017-1953-3) contains supplementary material, which is available to authorized users.

✉ Lin Tian  
xzittl@163.com

✉ Xiang E. Han  
xiangenh@163.com

<sup>1</sup> School of Chemical Engineering and Technology, China University of Mining & Technology, 221116 Xuzhou, China

<sup>2</sup> School of Chemical Engineering and Technology, Xuzhou Institute of Technology, 221018 Xuzhou, China

<sup>3</sup> School of Food Science and Technology, Xuzhou Institute of Technology, 221018 Xuzhou, China

<sup>4</sup> School of Chemical Engineering and Technology, Jiangsu Normal University, 221116 Xuzhou, China

## Introduction

Acridone derivatives not only possess excellent fluorescence properties (Swist and Soloduch 2013), but also exhibit a wide range of biological activities (Sathish et al. 2010). For example, several studies have shown that acridone derivatives exhibit potent inhibitory activities against a large number of biological targets, including cathepsins L and V (Marques et al. 2012) and acetylcholinesterases (Mohammadi-Khanaposhtani et al. 2015), as well as biological activity in several cell lines, including A549 lung carcinoma cells (Mouafo and Roy 2010) and CCRF-CEM cells (Cao et al. 2008). To prepare novel acridone derivatives with enhanced levels of activity and selectivity, researchers have directed significant efforts towards the design and synthesis of substituted acridone ring systems, and several interesting studies have emerged from this work (Tabarrini et al. 2006). In particular, acridone-4-carboxylic acid derivatives, such as the corresponding amides, have

been reported to exhibit enhanced levels of cytotoxicity towards a wide variety of cancer cells, compared with acridone alone (Wang et al. 2015).

However, there have been very few reports pertaining to the imine derivatives of acridone, where the amino group is directly linked to the 4-position of the acridone ring. With this in mind, we synthesized 11 novel Schiff base compounds based on the condensation of 4-aminoacridone with 11 different aldehydes. The 4-aminoacridone scaffold required for this work was efficiently synthesized following the optimization of conventional methods (Boyerl et al. 1991). The structures of all of the compounds synthesized in the current study were fully characterized using infrared ray (IR),  $^1\text{H}$ -nuclear magnetic resonance (NMR),  $^{13}\text{C}$ -NMR, and high-resolution mass spectrometry (HRMS). The X-ray crystal structure of compound **1g** was determined using X-ray crystallography. All of the Schiff base compounds prepared in the current study were screened in terms of their antitumor activities against several human cancer cell lines in vitro, including A549, HeLa, SGC-7901, and Raji cell lines. The results show that compound **1d** is potently cytotoxic against HeLa cells ( $\text{IC}_{50} = 7.75 \mu\text{M}$ ). We also performed quantitative structure–activity relationship (QSAR) studies for compounds exhibiting inhibitory activity against Raji cells, which resulted in a statistically significant CoMFA model with high predictive abilities ( $R^2_{\text{cv}} = 0.674$ ,  $R^2 = 0.952$ ).

Multidrug resistance (MDR) can lead to a decrease in the intracellular concentration of a drug, which can have an adverse impact on the therapeutic use and effectiveness of chemotherapeutic agents (Krishna and Mayer 2000). P-glycoprotein (P-gp), which is a plasma membrane protein and member of the ABC family of proteins, plays an important role in MDR (Kumar et al. 2014). It is noteworthy that acridone derivatives modulate MDR mechanisms that occur through ATP binding and transmembrane domain of P-gp (Zhang et al. 2015). Docking analysis was also used in the current study to identify the binding pattern of **1d** in the active site of P-gp, as well as evaluating the MDR modulatory potential of the other compounds.

## Material and methods

### Chemistry

All of the chemical reagents used in the current study were acquired from various commercial suppliers and purified using standard methods before being used. Melting points (M.p.) were determined using a digital M.p. apparatus (Shenke, Shanghai, China). IR spectra were recorded using a Bruker Alfer FT-IR spectrometer (Bruker, Karlsruhe, Germany).  $^1\text{H}$  NMR spectra were recorded in  $\text{DMSO}-d_6$  using a

Bruker DPX 400 MHz spectrometer. The chemical shifts ( $\delta$ ) have been reported in p.p.m. relative to tetramethylsilane, which was used as an internal reference. HRMS analyses were performed using a MicroTOF-Q spectrometer (Bruker). X-Ray crystal data were collected using a Bruker Smart APEX II CCD diffractometer. The chemical reactions were monitored using thin layer chromatography on silica gel plates and visualized with UV light.

### 2-[(2-Aminophenyl)amino]benzoic acid

A mixture of *o*-chlorobenzoic acid (6.23 g, 10 mmol), *o*-phenylenediamine (1.10 g, 10.1 mmol), anhydrous potassium carbonate (2.72 g, 20 mmol), and copper powder (240 mg) in dry *N,N*-dimethylformamide (DMF) (40 mL) was stirred for 8 h at 170 °C under an  $\text{N}_2$  atmosphere. The mixture was then cooled to room temperature and filtered to remove the copper powder. The filtrate was acidified to pH 1 with concentrated hydrochloric acid to give a precipitate, which was collected by filtration and purified by recrystallization from ethanol to give the desired product as a yellow solid in 90% yield. M.p.: 208.2–209.9 °C.  $^1\text{H}$  NMR (400 MHz,  $\text{DMSO}-d_6$ ):  $\delta$  9.04 (s, 1H), 7.86 (dd, 1H,  $J = 7.9$ , 1.6 Hz), 7.30 (dt, 1H,  $J = 7.2$ , 1.6 Hz), 7.04 (dd, 1H,  $J = 7.8$ , 1.6 Hz), 6.99 (dt, 1H,  $J = 7.8$ , 1.4 Hz), 6.83 (dd, 1H,  $J = 7.9$ , 1.2 Hz), 6.67 (dt, 1H,  $J = 7.9$  and 0.8 Hz), 6.63 (m, 2H).

### 4-Aminoacridone

2-[(2-aminophenyl)amino]benzoic acid (2.28 g) was subjected to a dehydration reaction in polyphosphoric acid (PPA; 60 mL) for 4 h at 120 °C. The reaction was then cooled to room temperature and poured into water (1000 mL). The resulting aqueous solution was neutralized (pH 7.0–8.0) by the addition of an aqueous solution of NaOH, resulting in the formation of a yellow precipitate. The precipitate was collected by filtration and washed with water, followed by petroleum ether, to give the crude product, which was recrystallized from EtOH to give the desired product as a yellow solid in 73% yield. M.p. 341.0–342.5 °C.  $^1\text{H}$  NMR (400 MHz,  $\text{DMSO}-d_6$ ):  $\delta$  10.63 (s, 1H), 8.22 (d, 1H,  $J = 9.2$  Hz), 7.74–7.70 (m, 1H), 7.67 (d, 1H,  $J = 7.6$  Hz), 7.54 (t, 1H,  $J = 4.4$  Hz), 7.03–7.02 (m, 2H), 5.56 (s, 2H).

### General procedure for the synthesis of the 4-aminoacridone Schiff bases

4-Aminoacridone (210 mg, 1.0 mmol) was added to absolute ethanol (20 mL), and the resulting mixture was stirred until it formed a solution. An aromatic aldehyde derivative (1.5 mmol) was then added to the solution in a dropwise manner, followed by two drops of acetic acid, and the resulting mixture was heated at reflux for 2–4 h. The

reaction mixture was then cooled to room temperature and evaporated at room temperature to produce a residue, which was purified using column chromatography over silica gel to give the crude product. The crude products were recrystallized from ethanol.

#### 4-(2-Hydroxybenzylideneamino)acridin-9(10H)-one (**1a**)

Isolated as a brown solid in 73% yield. M.p. 233.2–234.5 °C. IR (cm<sup>-1</sup>) 3394, 1621 ( $\nu_{\text{C=N}}$ ), 1624, 1335, 910, 744, 557. <sup>1</sup>H NMR (400 MHz, DMSO-*d*<sub>6</sub>):  $\delta$  11.60 (s, 1H), 10.93 (s, 1H), 9.03 (s, 1H), 8.27 (d, 1H, *J* = 7.2 Hz), 8.19 (d, 1H, *J* = 8.0 Hz), 7.98–7.95 (m, 2H), 7.76–7.73 (m, 1H), 7.60 (dd, 1H, *J* = 7.2 and 7.6 Hz), 7.51–7.46 (m, 1H), 7.32–7.27 (m, 2H), 7.06 (t, 1H, *J* = 7.6 Hz). <sup>13</sup>C NMR (125 MHz, DMSO-*d*<sub>6</sub>):  $\delta$  177.11(C=O), 163.63(C–OH), 160.00 (C=N), 141.24(C,C-10), 139.83(C,C-4), 135.74(C,C-2), 134.21(C,C-7), 133.76(C,C-18), 132.35(C,C-20), 126.28(C,C-11), 124.37(C,C-13), 122.53(C,C-6), 121.92(C,C-8), 121.72(C,C-1), 121.58(C,C-19), 121.18(C,C-15), 121.15(C,C-5), 119.77(C,C-12), 118.94(C,C-3), 117.06(C,C-17). HRMS: *m/z* 315.1134 for [M + H]<sup>+</sup>, calcd for C<sub>20</sub>H<sub>15</sub>N<sub>2</sub>O<sub>2</sub><sup>+</sup> = 315.1128.

#### 4-(Benzylideneamino)acridin-9(10H)-one (**1b**)

Isolated as a brown solid in 82% yield. M.p. 241.5–244.2 °C. IR (cm<sup>-1</sup>): 3449, 1625 ( $\nu_{\text{C=N}}$ ), 1623, 1477, 1449, 755, 688. <sup>1</sup>H NMR (400 MHz, DMSO-*d*<sub>6</sub>):  $\delta$  10.82 (s, 1H), 8.94 (s, 1H), 8.28–8.23 (m, 3H), 8.19 (d, 1H, *J* = 8.0 Hz), 8.06 (d, 1H, *J* = 8.0 Hz), 7.77–7.70 (m, 2H), 7.62–7.60 (m, 3H), 7.33–7.28 (m, 2H). <sup>13</sup>C NMR (125 MHz, DMSO-*d*<sub>6</sub>):  $\delta$  177.18(C=O), 161.96(C=N), 141.12(C,C-10), 139.72(C,C-4), 136.49(C,C-15), 136.43(C,C-2), 133.72(C,C-7), 132.40 (C,C-18), 130.24(C,C-11), 129.17(C,C-16=C-20), 126.29 (C,C-13), 124.43(C,C-17=C-19), 121.85(C,C-6), 121.75 (C,C-8), 121.47(C,C-1), 121.13(C,C-5), 120.98(C,C-12), 119.02(C,C-3). HRMS: *m/z* 299.1182 for [M + H]<sup>+</sup>, calcd for C<sub>20</sub>H<sub>15</sub>N<sub>2</sub>O<sup>+</sup> = 299.1179.

#### 4-(3-Methoxy-4-hydroxybenzylideneamino)acridin-9(10H)-one (**1c**)

Isolated as a brown solid in 87% yield. M.p. 216.5–219.6 °C. IR (cm<sup>-1</sup>): 3422, 1624 ( $\nu_{\text{C=N}}$ ), 1523, 1288, 755. <sup>1</sup>H NMR (400 MHz, DMSO-*d*<sub>6</sub>):  $\delta$  10.83 (s, 1H), 9.89 (s, 1H), 8.77 (s, 1H), 8.27 (d, 1H, *J* = 7.6 Hz), 8.12 (d, 1H, *J* = 7.2 Hz), 8.05 (d, 1H, *J* = 7.6 Hz), 7.92 (d, 1H, *J* = 1.6 Hz), 7.77 (t, 1H, *J* = 8.4 Hz), 7.65 (d, 1H, *J* = 7.2 Hz), 7.58 (dd, 1H, *J* = 8.4 Hz), 7.31–7.27 (m, 2H), 6.98 (d, 1H, *J* = 7.6 Hz), 3.96 (s, 3H). <sup>13</sup>C NMR (125 MHz, DMSO-*d*<sub>6</sub>):  $\delta$  177.24(C=O), 161.32(C=N), 151.28(C,C-18), 148.43(C,C-17), 141.04(C,C-10), 140.12(C,C-4), 136.45(C,C-10), 133.64(C,C-2),

128.35(C,C-7), 126.30(C,C-15), 125.84(C,C-11), 123.62(C,C-13), 121.77(C,C-6), 121.70(C,C-8), 121.10(C,C-20), 120.55(C,C-1), 119.07(C,C-5), 115.75(C,C-2), 112.36, 56.24(CH<sub>3</sub>–O). HRMS: *m/z* 345.1237 for [M + H]<sup>+</sup>, calcd for C<sub>20</sub>H<sub>17</sub>N<sub>2</sub>O<sub>3</sub><sup>+</sup> = 345.1234.

#### 4-(4-*N,N*-Dimethylbenzylideneamino)acridin-9(10H)-one (**1d**)

Isolated as a brown solid in 67% yield. M.p. 254.5–257.2 °C. IR (cm<sup>-1</sup>): 3417, 3322, 1639 ( $\nu_{\text{C=N}}$ ), 1608, 1508, 1474, 1395, 1250, 756, 656. <sup>1</sup>H NMR (400 MHz, DMSO-*d*<sub>6</sub>):  $\delta$  10.77 (s, 1H), 8.72 (s, 1H), 8.27 (d, 1H, *J* = 6.8 Hz), 8.09–8.04 (m, 4H), 7.76 (t, 1H, *J* = 8.4 Hz), 7.63 (d, 1H, *J* = 6.4 Hz), 7.30–7.25 (m, 2H), 6.88 (d, 2H, *J* = 9.2 Hz), 3.07 (s, 6H). <sup>13</sup>C NMR (125 MHz, DMSO-*d*<sub>6</sub>):  $\delta$  177.29 (C=O), 161.02(C=N), 153.23(C,C-18), 141.05(C,C-10), 140.59(C,C-4), 136.509(C,C-2), 133.589(C,C-7), 132.029 (C,C-11), 124.25(C,C-13), 122.96(C,C-16=C-20), 121.69 (C,C-6), 121.55(C,C-15), 121.07(C,C-8), 120.21(C,C-1), 119.05(C,C-5), 111.77(C,C-17=C-19), 79.64(C,CH<sub>3</sub>–N), 79.30(C,CH<sub>3</sub>–N). HRMS: *m/z* 342.1608 for [M + H]<sup>+</sup>, calcd for C<sub>20</sub>H<sub>20</sub>N<sub>3</sub>O<sup>+</sup> = 342.1601.

#### 4-(4-Bromobenzylideneamino)acridin-9(10H)-one (**1e**)

Isolated as a brown solid in 87% yield. M.p. 256.5–258.2 °C. IR (cm<sup>-1</sup>): 3412, 3224, 1620 ( $\nu_{\text{C=N}}$ ), 1598, 1569, 1523, 1483, 1449, 1341, 1066, 1008. <sup>1</sup>H NMR (400 MHz, DMSO-*d*<sub>6</sub>):  $\delta$  10.83 (s, 1H), 8.94 (s, 1H), 8.27 (d, 1H, *J* = 8.4 Hz), 8.21–8.17 (m, 3H), 8.05 (d, 1H, *J* = 8.4 Hz), 7.84 (d, 2H, *J* = 8.8 Hz), 7.78–7.72 (m, 2H), 7.33–7.28 (m, 2H). <sup>13</sup>C NMR (125 MHz, DMSO-*d*<sub>6</sub>):  $\delta$  177.17(C=O), 160.79 (C=N), 141.12(C,C-10), 139.35(C,C-4), 136.55(C,C-15), 135.63(C,C-2), 133.79(C,C-7), 132.26(C,C-11), 132.03(C,C-17=C-19), 126.31(C,C-13), 126.06(C,C-16=C-20), 124.74(C,C-6), 121.91(C,C-18), 121.81(C,C-8), 121.46(C,C-1), 121.14(C,C-5), 121.03(C,C-12), 119.00(C,C-3). HRMS: *m/z* 377.0287 for [M + H]<sup>+</sup>, calcd for C<sub>20</sub>H<sub>14</sub>BrN<sub>2</sub>O<sup>+</sup> = 377.0284.

#### 4-(4-Fluorobenzylideneamino)acridin-9(10H)-one (**1f**)

Isolated as a yellow solid in 76% yield. M.p. 205.2–208.2 °C. IR (cm<sup>-1</sup>): 3144, 3034, 1618 ( $\nu_{\text{C=N}}$ ), 1522, 1219, 1002, 836, 755. <sup>1</sup>H NMR (400 MHz, DMSO-*d*<sub>6</sub>):  $\delta$  10.83 (s, 1H), 8.95 (s, 1H), 8.28 (d, 1H, *J* = 8.4 Hz), 8.19 (dd, 1H, *J* = 8.8 Hz), 8.05 (d, 1H, *J* = 8.4 Hz), 7.78–7.67 (m, 4H), 7.33–7.28 (m, 2H). <sup>13</sup>C NMR (125 MHz, DMSO-*d*<sub>6</sub>):  $\delta$  177.18(C=O), 160.51(C=N), 141.10(C,C-10), 139.49(C,C-4), 136.51(C,C-2), 133.71(C,C-7), 132.67(C,C-15), 126.30(d, 1C, *J* = 56 Hz), 124.46(C,C-16=C-20), 121.83(C,C-11), 121.41(C,C-13), 121.12(C,C-6), 120.89(C,C-8), 118.97(C,C-5),

116.36(C,C-12), 116.14(C,C-3). HRMS:  $m/z$  317.1092 for  $[M + H]^+$ , calcd for  $C_{20}H_{14}FN_2O^+ = 317.1085$ .

#### 4-(2-Bromobenzylideneamino)acridin-9(10H)-one (**Ig**)

Isolated as a brown solid in 72% yield. M.p. 211.2–213.2 °C. IR ( $cm^{-1}$ ): 3064, 1619 ( $\nu_{C=N}$ ), 1561, 1523, 1477, 1340, 1261, 1183, 754, 675.  $^1H$  NMR (400 MHz, DMSO- $d_6$ ):  $\delta$  10.88 (s, 1H), 8.92 (s, 1H), 8.52 (s, 1H), 8.62 (dd, 1H,  $J = 7.6$  Hz), 8.28 (dd, 1H,  $J = 8.4$  Hz, 8.0 Hz), 8.21 (dd, 1H,  $J = 8.0$  and 8.4 Hz), 8.02 (d, 1H,  $J = 9.2$  Hz), 7.83 (d, 1H,  $J = 8.0$  Hz), 7.77–7.73 (m, 1H), 7.70 (dd, 1H,  $J = 8.0$  Hz), 7.66 (t, 1H,  $J = 7.6$  Hz), 7.58–7.54 (m, 1H), 7.34–7.28 (m, 2H).  $^{13}C$  NMR (125 MHz, DMSO- $d_6$ ):  $\delta$  177.11(C=O), 159.84(C=N), 141.14(C,C-10), 139.64(C,C-4), 136.44(C,C-15), 134.42(C,C-2), 134.07(C,C-17), 133.80(C,C-7), 133.70(C,C-11), 128.53(C,C-18), 126.30(C,C-13), 126.19(C,C-19), 125.06(C,C-20), 121.95(C,C-6), 121.79(C,C-8), 121.57(C,C-16), 121.31(C,C-1), 121.31(C,C-5), 121.17(C,C-12), 118.99(C,C-3). HRMS:  $m/z$  377.0287 for  $[M + H]^+$ , calcd for  $C_{20}H_{14}BrN_2O^+ = 377.0284$ .

#### 4-(3-Fluorobenzylideneamino)acridin-9(10H)-one (**Ih**)

Isolated as a yellow solid in 70% yield. M.p. 219.5–222.0 °C. IR ( $cm^{-1}$ ): 3022, 1629 ( $\nu_{C=N}$ ), 1525, 1348, 747, 551.  $^1H$  NMR (400 MHz, DMSO- $d_6$ ):  $\delta$  10.79 (s, 1H), 8.98 (s, 1H), 8.28 (dd, 1H,  $J = 8.0$  Hz), 8.23–8.18 (m, 2H), 8.06 (d, 1H,  $J = 8.0$  Hz), 8.00 (d, 1H,  $J = 7.6$  Hz), 7.79–7.75 (m, 2H), 7.69–7.64 (m, 1H), 7.50–7.45 (m, 1H), 7.34–7.29 (m, 1H).  $^{13}C$  NMR (125 MHz, DMSO- $d_6$ ):  $\delta$  177.20(C=O), 164.12(C-F), 161.70(C=N), 141.11(C,C-10), 139.03(C,C-4), 138.91(C,C-15), 136.63(C,C-2), 133.77(C,C-7), 131.23(C,C-19), 127.16(C,C-11), 126.31(C,C-13), 124.94(C,C-6), 121.83(C,C-20), 121.43(C,C-9), 121.13(C,C-5), 121.01(C,C-12), 119.29(C,C-3), 119.08(C,C-18), 115.57(C,C-16). HRMS:  $m/z$  317.1092 for  $[M + H]^+$ , calcd for  $C_{20}H_{14}FN_2O^+ = 317.1085$ .

#### 4-(3,4,5-Trimethoxybenzylideneamino)acridin-9(10H)-one (**Ii**)

Isolated as a yellow solid in 85% yield. M.p. 195.7–198.2 °C. IR ( $cm^{-1}$ ): 3431, 3385, 1685 ( $\nu_{C=N}$ ), 1587, 1505, 1463, 1392, 1331, 1234, 1128, 992, 846, 628.  $^1H$  NMR (400 MHz, DMSO- $d_6$ ):  $\delta$  10.86 (s, 1H), 8.85 (s, 1H), 8.28 (d, 1H,  $J = 9.6$  Hz), 8.17 (d, 1H,  $J = 9.2$  Hz), 8.04 (d, 1H,  $J = 8.4$  Hz), 7.72–7.30 (m, 1H), 7.68 (dd, 1H,  $J = 7.6$  Hz), 7.58 (s, 2H), 7.33–7.27 (m, 2H), 3.95 (s, 6H), 3.79 (s, 3H).  $^{13}C$  NMR (125 MHz, DMSO- $d_6$ ):  $\delta$  177.20(C=O), 161.40(C=N), 153.54(C,C-17=C-19), 141.31(C,C-10), 141.04(C,C-18), 139.65(C,C-4), 136.46(C,C-2), 133.71(C,C-11), 131.85(C,C-15), 126.31(C,C-7), 124.27(C,C-13), 121.85(C,

C-6), 121.49(C,C-8), 121.14(C,C-5), 120.76(C,C-12), 119.08(C,C-3), 107.64(C,C-16=C-20), 60.72(C,C-21=C-23), 56.58(C,C-22). HRMS:  $m/z$  389.1499  $[M + H]^+$ , calcd for  $C_{23}H_{21}N_2O_4^+ = 389.1496$ .

#### 4-(3,4-Dimethoxybenzylideneamino)acridin-9(10H)-one (**Ij**)

Isolated as a yellow solid in 83% yield. M.p. 187.3–189.2 °C. IR ( $cm^{-1}$ ): 3415, 3330, 1619 ( $\nu_{C=N}$ ), 1599, 1508, 1342, 1275, 1240, 1139, 1018, 860, 757, 636.  $^1H$  NMR (400 MHz, DMSO- $d_6$ ):  $\delta$  10.86 (s, 1H), 8.85 (s, 1H), 8.28 (d, 1H,  $J = 8.0$  Hz), 8.05 (d, 1H,  $J = 8.4$  Hz), 7.96 (d, 1H,  $J = 1.6$  Hz), 7.77–7.72 (m, 1H), 7.67–7.65 (m, 2H), 7.31 (t, 2H,  $J = 8.0$  Hz), 7.17 (d, 1H,  $J = 8.4$  Hz), 3.95 (s, 3H), 3.89 (s, 3H).  $^{13}C$  NMR (125 MHz, DMSO- $d_6$ ):  $\delta$  177.22(C=O), 161.24(C=N), 152.78(C,C-18), 149.43(C,C-17), 141.07(C,C-10), 139.95(C,C-4), 133.65(C,C-2), 129.48(C,C-7), 126.30(C,C-15), 125.73(C,C-11), 123.87(C,C-13), 121.78(C,C-6), 121.74(C,C-20), 121.48(C,C-8), 121.12(C,C-5), 120.66(C,C-12), 119.10(C,C-3), 111.64(C,C-16), 111.32(C,C-19), 56.13(C,C-21=C-22). HRMS:  $m/z$  359.1396 for  $[M + H]^+$ , calcd for  $C_{22}H_{19}N_2O_3^+ = 359.1390$ .

#### 4-(2,4-Dichlorobenzylideneamino)acridin-9(10H)-one (**Ik**)

Isolated as a yellow solid in 69% yield. M.p. 161.3–163.2 °C. IR ( $cm^{-1}$ ): 3417, 1647 ( $\nu_{C=N}$ ), 1523, 1473, 1295, 755.  $^1H$  NMR (400 MHz, DMSO- $d_6$ ):  $\delta$  10.85 (s, 1H), 9.10 (s, 1H), 8.68 (d, 1H,  $J = 8.4$  Hz), 8.27 (d, 1H,  $J = 8.0$  Hz), 8.21 (d, 1H,  $J = 6.0$  Hz), 8.01 (d, 1H,  $J = 8.8$  Hz), 7.84 (d, 1H,  $J = 6.0$  Hz), 7.76–7.67 (m, 3H), 7.34–7.28 (m, 2H).  $^{13}C$  NMR (125 MHz, DMSO- $d_6$ ):  $\delta$  177.09(C=O), 156.25(C=N), 141.11(C,C-10), 139.26(C,C-4), 137.64(C,C-2), 136.58(C,C-7), 136.54(C,C-15), 133.82(C,C-16), 132.12(C,C-11), 131.75(C,C-20), 129.93(C,C-13), 128.33(C,C-18), 126.31(C,C-6), 125.30(C,C-8), 121.96(C,C-5), 121.82(C,C-12), 118.95(C,C-3). HRMS:  $m/z$  367.0400 for  $[M + H]^+$ , calcd for  $C_{20}H_{13}Cl_2N_2O^+ = 367.0399$ .

### Single crystal cultivation and structure identification

Crystal growth and conditions: yellow crystals of **1g** suitable for X-ray crystallography were obtained at room temperature from an EtOH solution by slow evaporation of the solvent. The resulting crystals were then mounted on the goniometer of a single crystal diffractometer. Crystal data were collected at 296 K using Mo  $K\alpha$  radiation ( $\lambda = 0.710713 \text{ \AA}$ ) in the  $w/\nu$  scan mode and analyzed for Lorentz and polarization effects siemens area detector absorption. The structure was solved using the direct method and refined by full-matrix least-squares fitting on F2 using SHELX-97.

## Cytotoxicity assay against A549, Hela, SGC-7901, and Raji cell lines

Cells were cultured in RPMI-1640 medium with 10% fetal bovine serum, 100 U/mL of penicillin and 100 µg/mL of streptomycin in a 5% CO<sub>2</sub> humidified atmosphere at 37 °C. Cytotoxicity was evaluated using an MTT assay. Briefly, cells were seeded in 96-well tissue culture plates and incubated with compounds (0–100 µmol/L) for 48 h at 37 °C and 5% CO<sub>2</sub>. Following compound treatment, MTT (0.5 mg/mL) was added, and the resulting mixtures were incubated for 4 h. The reaction was then terminated by the removal of the supernatant and the remaining formazan crystals in each well were dissolved in 150 µL of DMSO. The optical density of each well was measured at 570 nm using a PowerWaveX Microplate Scanning Spectrophotometer (Bio-tek Instruments, Inc., Vermont, America). The percentage inhibition of cell proliferation of each compound was then calculated at various concentrations.

## 3D-QSAR studies

The 11 compounds generated in the current study were divided into training and testing sets including compounds **1c** and **1i**, respectively. The testing set compounds were randomly selected. The inhibition ratio values were converted into logarithmic values (inhibition ratio × 100) for the QSAR study. The three-dimensional (3D) structures of these compounds were built using the SYBYLx2.0 software (Tripos, SaintLouis, America). Partial atomic charges were calculated using the Gasteiger–Huckel method, and energy minimizations were performed using the Tripos force field and the Powell conjugate gradient algorithm with a convergence criterion of 0.001 kcal/mol. The steric and electrostatic interaction fields for CoMFA were calculated using the default parameters from SYBYL: 2.0 kcal/mol grid point spacing, sp<sup>3</sup> carbon probe atom with +1 charge and a van der Waals radius of 1.52 Å, and column filtering of 2.0 kcal/mol. The descriptors calculated from the CoMFA analysis were used as independent variables and the experimental logarithmic 100 × inhibition ratio (lgIR) values were used as dependent variables in a partial least-squares (PLS) analysis to derive the 3D-QSAR model. Leave-one-out cross-

validation and the SAMPLS program were used to obtain the optimal number of components (Noc) and cross-validated coefficient ( $R^2_{cv}$ ). After the optimal Noc was determined, anon-cross-validated analysis was performed without column filtering to obtain the regression coefficients ( $R^2$ ), which determine the external predictive ability.

## Molecular docking

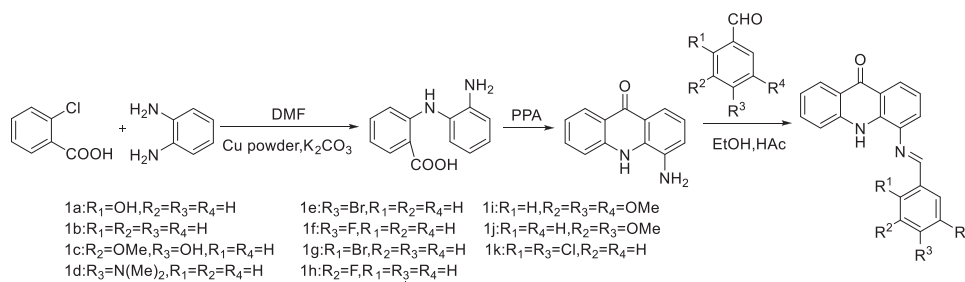
The 3D structures of P-gp (PDB ID: 1MV5 and 3G60) were downloaded from the Protein Data Bank (<http://www.rcsb.org/pdb/home/home.do>). The 3D structures of **1d** were drawn using the ChemBioDraw Ultra 12.0 and ChemBio3D Ultra 12.0 software packages (CambridgeSoft, MA, USA). The AutoDockTools 1.5.6 package (<http://mgltools.scripps.edu>) was used to generate the docking input files. The search grid for the transmembrane binding site of P-gp was identified as center\_x: 19.133, center\_y: 52.68 and center\_z: 0.174 with dimensions of size\_x: 15, size\_y: 15 and size\_z: 15, whereas the search grid for the ATP binding site of P-gp was identified as center\_x: 3.091, center\_y: 52.697 and center\_z: 107.494, with dimensions of size\_x: 15, size\_y: 15 and size\_z: 15. The value of exhaustiveness was set at 20. The default parameters were used for the Vina docking experiments. The best-scoring pose as judged by the Vina docking score was chosen and visually analyzed using version 1.7.6 of the PyMOL 1.7.6 (<http://www.pymol.org/>).

## Results and discussion

### Chemistry

The target compounds were synthesized as outlined in Scheme 1. The properties of acridone derivatives have traditionally been difficult to evaluate because of the lack of an efficient synthetic method for the construction of these compounds. Many scientists have obtained satisfactory results through the development of novel synthetic methods (Shi et al. 2013). Using a conventional method, compound **1** was synthesized in DMF in the absence of a nitrogen protecting group in 83% yield, and 4-aminoacridone was synthesized in the strong oxidizing/dehydrating agent

**Scheme 1** Synthesis of 4-aminoacridone and its derivatives (yields: 67–87%)



H<sub>2</sub>SO<sub>4</sub> with a low yield of 31% (Boyerl et al. 1991). To provide reliable access to large quantities of 4-aminoacridone, we investigated the optimization of the experimental conditions. The results of a series of screening experiments revealed that the initial reaction of 2-chlorobenzoic acid with benzene-1,2-diamine in the presence of copper powder and potassium carbonate in DMF gave the S<sub>N</sub>Ar product 2-[(2-aminophenyl)amino]benzoic acid with an isolated yield of up to 90%. The subsequent dehydration of 2-[(2-aminophenyl)amino]benzoic acid in the presence of the mild dehydrating agent PPA, resulted in the formation of 4-aminoacridone in a much higher isolated yield of 73% whilst avoiding the need for a strongly oxidizing dehydration reagent. The Schiff bases were synthesized using a conventional condensation method. The X-ray crystal structure of **1g** was solved and it clearly shows the desired Schiff base functional group (Fig. 1).

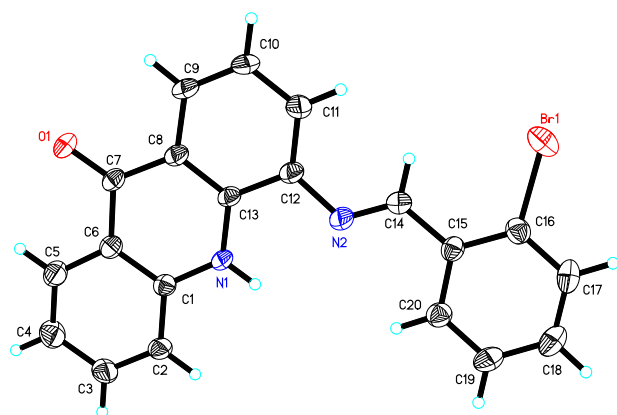


**Fig. 1** X-Ray crystal structure of compound **1g**

## Biological activity

All of the Schiff base compounds (**1a–k**) synthesized in the current study and 4-aminoacridone were evaluated to determine their cytotoxicity against several human cancer cell lines, including A549, HeLa, SGC-7901, and Raji cells. Cisplatin was used as a positive control. These experiments revealed that most of these Schiff bases exhibit potent cytotoxicity towards HeLa and Raji cells. However, only a few compounds exhibited cytotoxicity towards A549 cells, with most compounds also showing low activity against SGC-7901 cells. The results of these experiments are summarized in Table 1, where the activities of the different compounds are presented as inhibition ratios and IC<sub>50</sub> values.

As shown in Table 1, compound **1d** exhibited the highest activity of all of the compounds tested against the HeLa cells, with an IC<sub>50</sub> value of 7.75 μM. In contrast, compounds **1a** and **1k** showed lower levels of activity, with IC<sub>50</sub> values greater than 30 μM. Compounds **1c**, **1e**, **1f**, and **1i** also showed weak activity against HeLa cells. Analysis of the structure–activity relationships for these compounds revealed that the nature of the substituent groups on the phenyl ring has a pronounced effect on their activities against HeLa cells. For example, compounds such as **1d**, **1k**, **1a**, and **1c**, bearing a Cl, OH, or N(Me)<sub>2</sub> group at R<sub>1</sub> or R<sub>3</sub> displayed greater cytotoxicity. Compound **1k**, bearing a 2,4-dichlorosubstituted phenyl ring or compound **1d**, bearing a larger –N(Me)<sub>2</sub> substituent at the 4-position of its phenyl ring, exhibited potent activity against HeLa cells. However, these two compounds showed much weaker activities against the other three tested cell lines, highlighting their selectivity for HeLa cells.

**Table 1** Antitumor activities (μmol/L) of the Schiff base derivatives of 4-aminoacridone

Compd	A549		HeLa		SGC-7901		Raji	
	Inhibition ratio (%)	IC <sub>50</sub> (μM)						
Cisplatin		5.34		4.62		2.27		5.20
4-AA <sup>a</sup>	22.41		41.02		25.23		47.60	
<b>1a</b>	21.27		71.33	24.0	28.42		56.73	63.21
<b>1b</b>	42.43		13.74		34.02		46.00	
<b>1c</b>	34.14		66.02	36.50	0.67		62.65	64.77
<b>1d</b>	39.55		95.61	7.75	0.74		82.13	62.21
<b>1e</b>	65.11	48.12	74.36	56.62	44.26	104.25	62.65	63.96
<b>1f</b>	44.50		78.24	52.5	8.43		30.63	
<b>1g</b>	76.70	35.64	32.37		75.58	53.13	34.00	
<b>1h</b>	45.18		54.41	82.62	22.97		33.00	
<b>1i</b>	26.99		66.69	59.5	/		67.49	60.86
<b>1j</b>	33.30		43.12		/		60.27	73.41
<b>1k</b>	77.28	45.48	76.26	8.88	63.39	72.63	61.65	87.03

<sup>a</sup> Expressed 4-aminoacridone

### 3D-QSAR analysis

The majority of the Schiff base compounds synthesized in the current study exhibit better antitumor activity towards the HeLa and Raji cells than other cells. Consequently, a QSAR study on the biological testing data for the HeLa and Raji cells was performed. However, a very low regression coefficient ( $R^2$ ) was obtained for the HeLa cells, although a better result was obtained for the Raji cells. A fragment of the structure of compound **1d** was used as a template to align the other compounds. The statistical results of the 3D-QSAR model show that the cross-validated correlation coefficient  $R^2_{cv} = 0.719 > 0.5$ , corresponding to  $N_{oc} = 3$ , whereas the 3D-QSAR of the non-cross-validated model gave  $R = 0.952$ ,  $S_E = 0.081$ , and  $F = 46.497$ . These results indicate that the model provided good correlation and accuracy characteristics for prediction of the compound activities. The contributions of the steric and electrostatic fields in the 3D-QSAR model were 58.8 and 41.2%, respectively.

All of the synthesized compounds were randomly divided into two groups: **1c** and **1i** were used as a testing set, whereas the remaining nine compounds were used as a training set. PLS analysis was also conducted using compound **1b** from the training set as a template for all of the other compounds. The results of this analysis were  $R^2_{cv} = 0.674 > 0.5$ ,  $N_{oc} = 3$ . The 3D-QSAR of the non-cross-validated model gave  $R = 0.956$ ,  $S_E = 0.040$  and  $F = 36.588$ . It is clear from these results that the estimated values are very similar to the test values.

Therefore, these results indicate that the CoMFA model has a good predictive capability. The predicted lgIR values are generally in good agreement with the experimental data (Table 2). The results of the CoMFA indicate that the contributions of the steric and electrostatic fields in the 3D-QSAR model are 64.2 and 35.8%, respectively. The steric and electrostatic contribution contour maps of the model are depicted in Fig. 2. The 3D contour maps show that changes in the molecular fields are associated with differences in biological activity. The *green* and *yellow* areas show the steric fields, whereas the *green* contour regions suggest that the introduction of larger substituents at these positions would lead to an improvement in the biological activity. Finally, the *yellow* region indicates that the introduction of a bulky group would have an adverse impact on the inhibitory activity.

As shown in the steric contour map (Fig. 2a), the *green* contour around  $R_3$  indicates that the introduction of a bulky group at this position would lead to an increase in biological activity. For example, compounds **1d**, **1e**, and **1f** bearing a  $-N(CH_3)_2$ ,  $-Br$  or  $-F$  substituent at the 4-, 5-, or 6-position of their phenyl ring, respectively, show better inhibitory activity than compound X, bearing a hydrogen atom at the 2

**Table 2** lgIR (logarithmic  $100 \times$  inhibition ratio) of the Schiff bases of 4-aminoacridone against Raji cells

compd.	lgIR			compd.	lgIR		
	exp.	cal.	err.		exp.	cal.	err.
<b>1a</b>	1.754	1.781	-0.027	<b>1g</b>	1.531	1.550	-0.019
<b>1b</b>	1.663	1.617	0.046	<b>1h</b>	1.519	1.489	0.030
<b>1c</b>	1.797	1.718	0.079	<b>1i</b>	1.829	1.805	0.024
<b>1d</b>	1.915	1.918	-0.003	<b>1j</b>	1.780	1.780	0.000
<b>1e</b>	1.797	1.767	-0.030	<b>1k</b>	1.790	1.794	-0.004
<b>1f</b>	1.486	1.539	-0.053				

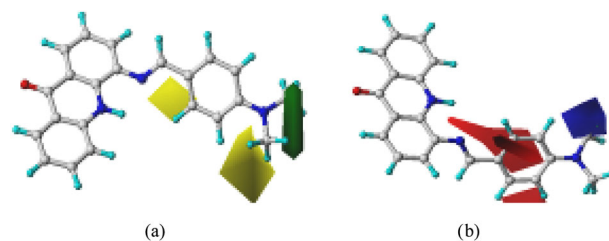


**Fig. 2** CoMFA contour maps: **a** steric contour map **b** electrostatic contour map

position of its phenyl ring. The two *yellow* contours around the  $R_1$  and  $R_2$  positions indicate that the introduction of small groups at these positions would lead to an improvement in their activity. The CoMFA electrostatic fields in *blue* show the regions where the occurrence of a positive charge would lead to an increase in activity, whereas the *red* regions indicate the areas where the introduction of negatively charged groups would be favorable.

In the electrostatic map (Fig. 2b), the two red contours around  $R_1$  and  $R_4$  indicate that the introduction of electronegative groups at these positions would lead to an increase in biological activity, especially at the  $R_1$  position. The small blue contours surrounding the  $R_3$  substituent suggest that the introduction of an electropositive group would increase activity at the 3-position, whereas the *red* contour at the 1-position indicates that the introduction of electronegative groups at this position would also be favorable for increased activity.

Analysis of compound **1d**, which exhibits the greatest activity of all the compounds tested against Raji cells, revealed that it has a large electropositive  $-N(CH_3)_2$  group at the 4-position of its phenyl ring and small groups ( $-H$ ) at the 2, 3, 5, and 6 positions of the same ring, which conforms to the steric and electrostatic contribution contour maps. In contrast, compound **1f**, with a small electronegative group ( $-F$ ) at the 4-position of its phenyl ring, did not match the model, and has the weakest activity. Based on the CoMFA model, it is envisaged that the introduction of a large electropositive group at the 4-position, together with a small electronegative group at the 2-position would improve

biological activity. The synthesis of such an optimized compound will be the focus of future work.

### Docking analysis

Acridone derivatives have been reported to modulate MDR by binding to the ATP and transmembrane domains of P-gp (Zhang et al. 2015). To reveal the MDR modulatory activity and binding behavior of compound **1d**, we conducted molecular docking studies to investigate the binding mode of **1d** to P-gp using Autodock vina 1.1.2. The docking of compound **1d** into the transmembrane binding pocket led to the formation of much better interactions compared with the ATP binding pocket.

The theoretical binding mode of **1d** to the transmembrane binding site of P-gp is shown in Fig. 3. The acridone scaffold of **1d** binds at the bottom of the pocket, where it forms a series of high density van der Waals contacts, whereas the *N,N*-dimethylphenyl group of **1d** is located in a hydrophobic pocket, surrounded by residues Ala-981, Ile-336, Met-68, and Tyr-949. Detailed analysis shows that two  $\pi$ - $\pi$  stacking interactions are present between the acridone scaffold and the side chains of residues Phe-728 and Phe-974. In addition, the phenyl group at the 10-position of the acridone scaffold forms a  $\pi$ - $\pi$  interaction with the side chain of the Phe-332 residue. Importantly, the carbonyl oxygen atom of the acridone core in **1d** forms an essential hydrogen bond with the Ser-975 residue, which is the main interaction between **1d** and P-gp.

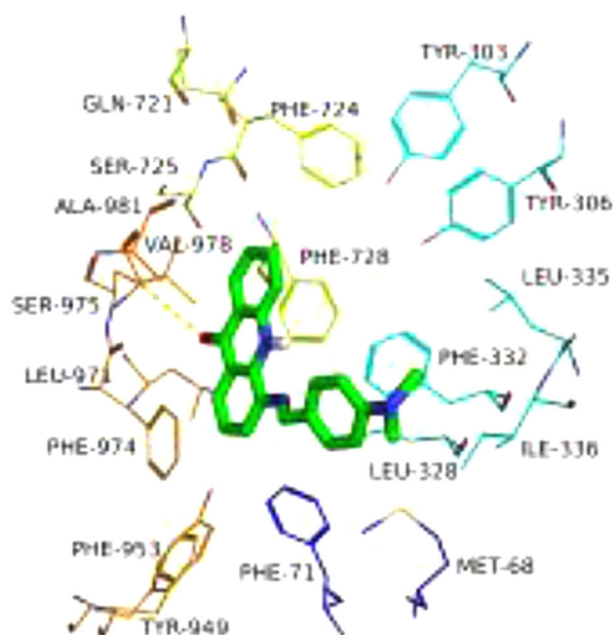


**Fig. 3** PyMol image for the docking of compound **1k** into the transmembrane binding site of P-gp

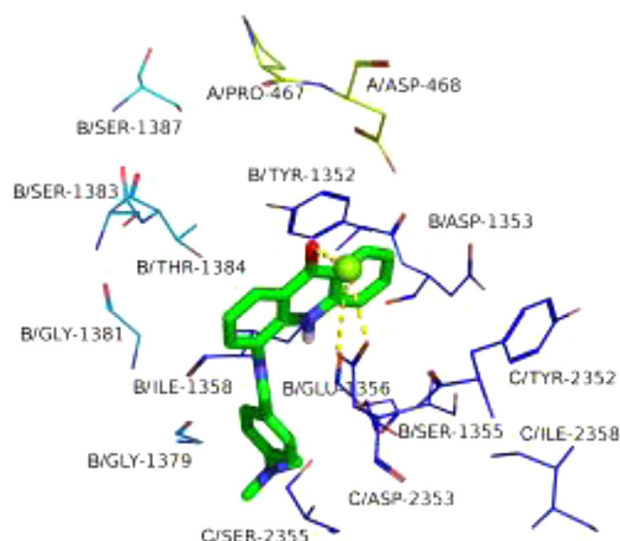


**Fig. 4** PyMol image for the docking of compound **1k** into the ATP binding site of P-gp

Compound **1d** docks into the ATP binding site of P-gp and the theoretical binding mode between **1d** and P-gp is shown Fig. 4. The acridone scaffold of **1d** binds at the entrance to the pocket, where it forms a high density of van der Waals contacts, whereas the *N,N*-dimethylphenyl moiety of **1d** is located at the bottom of the pocket, surrounded by residues B/Glu-1356, B/Ile-1358, B/Gly-1379, and C/Ser-2355. A detailed analysis showed that one of the phenyl rings of the acridone core displays  $\pi$ - $\pi$  stacking interactions with the B/Tyr-1352 and C/Tyr-2352 amino acid residues. Importantly, the carbonyl oxygen atom of the acridone ring in **1d** forms a series of essential coordination interactions with  $Mg^{2+}$ , which is chelated by residue C/Asp-2353.

### Conclusion

We have developed an optimized route for the synthesis of 4-aminoacridone based on conventional methods. This material was subsequently used to prepare a series of Schiff bases (**1a-k**), which were screened against several human cancer cell lines to evaluate their antitumor activity. Notably, compounds **1d** and **1k** displayed potent antitumor activity against HeLa cells. These data were used to generate a CoMFA model with  $R^2_{cv} = 0.674$  and  $R = 0.956$ . The low standard error of estimation and the high F values confirm that this CoMFA model possesses a significant prediction ability. The model predicts that the introduction of a large electropositive group at the 4-position of 4-aminoacridone, as well as a small electronegative group added to the 1,4-position, would lead to an improvement in the activity against Raji cells. Docking analysis indicates that **1d** forms stronger interactions with the transmembrane

binding pocket of P-gp than it does with the P-gp ATP binding site, indicating that it could act as an MDR inhibitor. Based on this analysis, it can be concluded that compound **1d** exhibits significant anti-cancer activity in addition to its predicted effects against MDR.

**Acknowledgements** Lin Tian thanks Gui F. Dai, Zhengzhou University, Zhengzhou, for testing the activity of the compounds. The authors thank the Chinese National Natural Science Foundation (31270577).

#### Compliance with ethical standards

**Conflict of interest** The authors declare that they have no competing interests.

#### References

- Boyerl G, Galy J, Barbe J (1991) [Synthèse et caractérisation de bis acridines pontées en positions 2, 3 ou 4]. *J Heterocycl Chem* 28:913–918
- Cao DR, Gao CM, Jiang YY, Tan CY (2008) Synthesis and potent antileukemic activities of 10-benzyl-9(10H)-acridinones. *Bioorg Med Chem* 16:8670–8675
- Krishna R, Mayer LD (2000) Multidrug resistance (MDR) in cancer: mechanisms, reversal using modulators of MDR and the role of MDR modulators in influencing the pharmacokinetics of anticancer drugs. *Eur J Pharm Sci* 11:265–283
- Kumar R, Bahia MS, Silakari O (2014) Synthesis, cytotoxic activity, and computational analysis of *N*<sup>10</sup>-substituted acridone analogs. *Med Chem Res* 24:1–13
- Marques EF, Bueno MA, Duarte PD, Vieira PC, Corrêa AG (2012) Evaluation of synthetic acridones and 4-quinolinones as potent inhibitors of cathepsins L and V. *Eur J Med Chem* 54:10–21
- Mohammadi-Khanaposhtani M, Saeedi M, Shafiee A, Akbarzadeh T (2015) Potent acetylcholinesterase inhibitors: design, synthesis, biological evaluation, and docking study of acridone linked to 1,2,3-triazole derivatives. *Eur J Med Chem* 92:799–806
- Mouafo RM, Roy R (2010) *In vitro* cytotoxic activity of isolated acridones alkaloids from *Zanthoxylum lepreurii* Guill. et Perr. *Bioorg Med Chem* 18:3605
- Sathish NK, GopKumar P, Prasad VVSR, Kumar SMS, Mayur YC (2010) Synthesis, chemical characterization of novel 1,3-dimethyl acridones as cytotoxic agents, and their DNA-binding studies. *Med Chem Res* 19:674–689
- Shi F, Zhu RY, Liang X, Tu SJ (2013) Catalytic asymmetric 1,3-dipolar cycloadditions of alkynes with isatin-derived azomethine ylides: enantioselective synthesis of spiro[indoline-3,2'-pyrrole] derivatives. *Adv Synth Catal* 355:2447–2458
- Swist A, Soloduch J (2013) Novel acridone-based branched blocks as highly fluorescent materials. *Syn Met* 18:1–8
- Tabarrini O, Dutartre H, Paeshuysse J, Neyts J (2006) Synthesis and anti-BVDV activity of acridones as new potential antiviral agents. *J Med Chem* 49:2621–2627
- Wang XQ, Xia CL, Huang ZS (2015) Design, synthesis, and biological evaluation of 2-arylethenylquinoline derivatives as multifunctional agents for the treatment of Alzheimer's disease. *Eur J Med Chem* 89:349–361
- Zhang B, Chen K, Wang N, Liu HX, Jiang YY (2015) Molecular design, synthesis and biological research of novel pyridyl acridones as potent DNA-binding and apoptosis-inducing agents. *Eur J Med Chem* 93:214–226